Journal of Materials Chemistry A

ROYAL SOCIETY OF CHEMISTRY

COMMUNICATION

View Article Online
View Journal | View Issue

Cite this: J. Mater. Chem. A, 2024, 12, 8683

Received 18th December 2023
Accepted 9th March 2024

DOI: 10.1039/d3ta07840j

rsc.li/materials-a

Effect of salt selection and molar ratio in molten salt synthesis of single-crystalline $LiNiO_2$†

Wessel van den Bergh,*[a] Rui Yao,[a] Ruizhuo Zhang,[a] Aleksandr Kondrakov,[ab] Jürgen Janek[ac] and Torsten Brezesinski*[a]

Single crystal (SC) layered lithium metal oxides ($LiNi_xCo_yMn_zO_2$, referred to as NCMs or NMCs) represent a new material design with unique benefits compared to their polycrystalline counterparts. However, preparation of SC-NCMs remains challenging, with methods such as molten salt synthesis being largely dependent on recipe-by-recipe reporting and no overarching conception of how to prepare desirable materials. For a model NCM, $LiNiO_2$ (LNO), we use experimental design methodology to identify how the factors of salt selection, salt mixtures, and molar salt ratio affect the critical features of grain size, crystal defect content ($Ni_{Li}^{\cdot}$), and particle size distribution. Herein, we identify that NaCl and KCl are salts which can be used to control particle size at relatively low defect content, while sulfate-containing salts are deleterious to quality LNO. The results of this work set out to provide a more comprehensive understanding of how others could prepare well-ordered SC-NCMs of specific particle size.

Li-ion energy storage developments proceed in the context of increasing societal implementation,[1–3] and as a hopeful aid to mitigate our contributions to climate change.[4,5] These developments seek to close the gaps of energy density and rate capability (charge time) with much of this focus on the positive electrode (cathode), as it is the most expensive component in a battery.[6,7] Commercial battery systems are transitioning away from the original $LiCoO_2$ (LCO)[8,9] first used in 1991 to greater fractions of Mn and Ni ($LiNi_xCo_yMn_zO_2$, NCM or NMC) for higher capacity, reduced material cost, and minimization of ethical compromise.[10–14] One direction of development is towards high Ni systems. $LiNiO_2$ (LNO) represents an endmember of the NCM system with a high theoretical specific capacity of 274 mA h g^{-1},[15] however at the expense of electrochemical,[16,17] mechanical,[18,19] and thermal stability.[20] Despite its current inadequacy as a commercial cathode material, LNO does represent a model platform for troubleshooting issues common to NCMs. Parallel to this, commercial systems utilize polycrystalline (PC) particles, which when paired with liquid electrolyte show degradation[21,22] and have safety issues[23,24] that would require new battery designs to avoid. Solid-state batteries (SSBs), which use superionic solid electrolytes, present a means to avoid those hazards, yet PC particles' porous character prevents complete contact with solid electrolyte, resulting in poor performance.[25–27] In contrast, single crystal (SC) particle morphologies are well suited to a solid-state design.[25,28–30] As a matter of definition for the materials herein,[31] SC refers to particles with minimal agglomeration (3–5 crystallites) as opposed to PC particles, which are composed of hundreds of crystallites (primary particles), and the intermediate condition of quasi-single crystalline. Regardless, SC materials are relatively new, as PC preparation is much more facile (as of writing). With this in mind, developing the best synthetic techniques for SC-LNO would give insights for how others can ultimately implement SSBs *en masse*.

Both SC synthesis and different emphasis on critical material parameters distinguish themselves from established PC methods. Using LNO as an example, the "traditional" synthesis consists of mixing $Ni(OH)_2$ and a modest excess (1.0 : 1.01–1.0 : 1.05) $LiOH \cdot H_2O$ (lithium carbonate is more common for NCMs of medium Ni content), followed by a pre-annealing/lithiation step at 400–550 °C for a few hours before ramping to 650–750 °C for 6–20 h. Depending upon the excess $LiOH \cdot H_2O$ used and presence of surface residuals, this may be washed and re-annealed to remove the introduced and intercalated protons (Li^+/H^+ exchange).[32]

SC synthesis has three different approaches to preparation,[31] each with their benefits and challenges to scalable application. High-temperature methods[33–36] utilize increased sintering kinetics to produce SC materials, however at the cost of

[a]Battery and Electrochemistry Laboratory (BELLA), Institute of Nanotechnology, Karlsruhe Institute of Technology (KIT), Herrmann-von-Helmholtz-Platz 1, 76344 Eggenstein-Leopoldshafen, Germany. E-mail: wessel.j.vdb@gmail.com; torsten.brezesinski@kit.edu

[b]BASF SE, Carl-Bosch-Str. 38, 67056 Ludwigshafen, Germany

[c]Institute of Physical Chemistry & Center for Materials Research (ZfM/LaMa), Justus-Liebig-University Giessen, Heinrich-Buff-Ring 17, 35392 Giessen, Germany

† Electronic supplementary information (ESI) available. See DOI: https://doi.org/10.1039/d3ta07840j

agglomeration and high defect content that require additional steps to rectify.[33,35] Multistep approaches[37–39] use differences in growth kinetics of specific phases or other material discrepancies to produce SC materials, however through sometimes lengthy procedures with little unifying concept for what each step in the process can truly contribute. Lastly, there is the molten salt methodology[40–45] discussed in this work. Molten salts for NCMs use lithium-contributing reagents and/or inactive spectator ions to grow crystallites *via* both sintering and Ostwald ripening.[46] Single crystals can be prepared in a single step at relatively low temperatures foregoing some of the aforementioned issues with other methods. The downside is that molten salt methods do require a washing step to remove the salts and, for Ni-rich samples, an additional annealing step. Many SC NCM molten salt syntheses have been reported with compelling electrochemical performance and some control over size and crystal habit (shape), with some effort to systematize the underlying contributions to what yields the "best" material.[31,40] However, this body of work is still dominated by recipe-by-recipe reporting, with no through line as to how molten salts can prepare specific features, such as size and morphology. This represents a serious barrier to accelerated innovations on SC-NCM synthesis. In this work, we report the first systematic examination of molten salt synthesis of SC-LNO using design of experiments (DoE) methodology.

Molten salt synthesis is an established method in traditional inorganic disciplines, yet requires detailed consideration in the context of NCMs given their synthetic restrictions. Inorganic synthesis of oxides, for example, has a massive design space with temperatures ranging from 300 to 1500 °C, using anything from fluoride to oxide fluxes at a molar ratio of 10 : 1 as a starting point, all while using a sealed vessel under synthetic conditions that deem 1 °C min^{-1} to be a very fast ramp rate.[47] This contrasts with NCM synthesis, which typically resides between 600 and 900 °C under flowing oxygen that should take less than a day to complete. This constrains conditions with which desirable SC materials can be made. Therefore, any salts used in synthesis must meet the following conditions: first, the salts or their eutectic(s) must have a sufficiently low melting point to function; second, the salt(s) must either act as a lithium source or be chemically inert to the formation of NCM, *i.e.* no insertion of spectator ions; third, the salt(s) must be very soluble in water to make the unavoidable post-processing practical; and fourth, the salt(s) should be cheap as innovations with expensive reagents relegates it to academic curiosity and niche applications. With these conditions in mind, preliminary exploration of the FTsalt – FACT salt phase diagram database yielded the chosen salts shown in Scheme 1 for synthesis of our "model" NCM (LNO). Na^+ has literature precedent, indicating it is non-reactive to NCMs.[44,45] Because of the greater ionic radii of K^+ and Cs^+, the same was assumed for all salts used. While CsCl is prohibitively expensive for large-scale use, it served as an additional component (point) in the mixture design to determine what effect cationic radius would have on desired features. K_2SO_4 and Na_2SO_4 were included, however they have melting points at an excess of 1069 and 884 °C and therefore deemed unwieldy as pure salt melts.

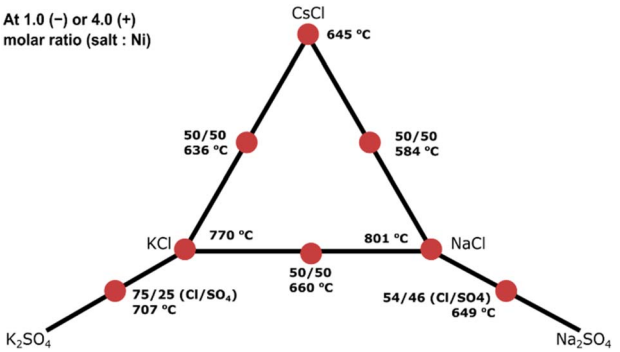

Scheme 1 A visual representation of the *D*-optimal experimental design produced with each point representing a mixture condition.

Nevertheless, they substantially suppress the melting point as eutectics with their respective chlorides. Experiments with other candidates, such as $CaCl_2$ and $MgCl_2$, resulted in a failure to form *R*–3*m* LNO. Additionally, we selected for a molar ratio (salt to Ni) from 1.0 to 4.0 that felt could be scaled synthetically and still yield single crystals. With all these preliminaries considered, a *D*-optimal (16 run) design was prepared consisting of a two-level factor for molar ratio of salt to Ni and mixture design of the salts, with exclusions to binary mixtures that had reported melting points, as presented in Scheme 1 (a complete list of samples can be found in Table S1†). Three responses were examined: particle size at the 50th percentile of the population (d_{50}, μm) and particle size dispersity, which were determined by scanning electron microscopy (SEM) image analysis (details in ESI and Fig. S1†), as well as point defects of Ni in the Li layer (Wyckoff 3b) as determined by Rietveld refinement (see Tables S2 and S3†). All calcinations were done using the same furnace with a 520 °C pre-annealing step and 880 °C calcination under 25 L h^{-1} of O_2 (>25 atm h^{-1}). While these calcination temperatures are well above what is standard for LNO synthesis, such extreme conditions allow for greater statistical contrast in sizes between samples. Further experimental details can be found in the ESI.† All runs were used in the analyses except for that whose conditions used a mixture of NaCl and Na_2SO_4 at 4.0 mol equivalents to $Ni(OH)_2$ for reasons that are discussed below.

Particle size of a cathode material is a critical feature that ultimately dictates the electrochemical performance and can be controlled by proper proportion of salts. On a theoretical level, basic models note a square dependence upon the path length a species must travel and the time it takes to do so.[48–50] Crystallite size (roughly equivalent to particle/grain size in SC systems) has been observed to be a critical feature experimentally.[51–53] Furthermore, the relative ratio of material that is subject to surface-based reactions and material in the "bulk" depends upon particle size as well, leading to an often overlooked relationship between particle size and material stability.[54] Fig. 1 shows two representative samples, CsCl(−), which refers to a synthetic condition of 1.0 mol equivalent or "(−)" of CsCl to $Ni(OH)_2$ and KCl–NaCl(+), which refers to a 50 : 50 mixture of KCl and NaCl at a total molar equivalent of 4.0 "(+)" to 1.0 mol of $Ni(OH)_2$. A notable difference can be observed

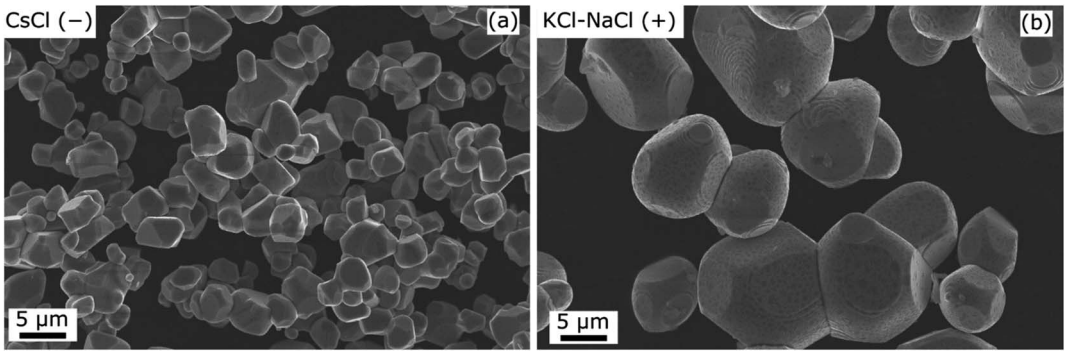

Fig. 1 SEM images of representative samples, (a) CsCl(−) and (b) KCl–NaCl(+). SEM images of other representative samples can be found in Fig. S2–S19.†

in particle size and distinguishing features in morphology, where CsCl(−) loosely consists of flat intersecting facets to make up the particle, while KCl–NaCl(+) demonstrates flat facets, which meet curved surfaces that have terracing. Terracing was observed in NaCl and CsCl–NaCl as well. One possible explanation for this unique feature is that terracing minimizes surface energy by reducing the number of surface step atoms.[55] With regards to other differences in crystal habit, the proper analysis and assignment of observed morphologies to theoretical ones are subject of future work. Regardless, analysis of variance (ANOVA) of the d_{50} particle size data (see Fig. 2) reduced a broad range of factors and interactions down to five statistically significant terms, three main effects and two second-order interactions, which are represented as terms in the linear model shown in the equation below (see also Table 1). To articulate the model, the findings can be broken down into simple concepts. The molar salt ratio is a significant factor that indicates greater additions of salt yield larger particles. Greater fractions of NaCl in a mixture yield greater particle sizes, so in theory, a binary mixture of NaCl and CsCl (insignificant factor, however whose estimate in the model is similar to KCl, as evidenced by Fig. 2) can be a means to achieve select particle sizes between around 4 and 11 μm by salt choice alone. KCl, in context of the model, yields much smaller particles and does not promote substantial growth like NaCl. Rather, there is a significant interaction between KCl and NaCl, where presence of the two suppresses particle growth, which contrasts with the interaction between KCl and K_2SO_4, having a positive effect on particle size. However, for reasons noted later on, sulfate-based salts seem to be a poor choice for overall material quality. These significant factors can be represented as the following equation:

$$d_{50} = \beta_{\mathrm{NaCl}}(f_{\mathrm{NaCl}}) + \beta_{\mathrm{KCl}}(f_{\mathrm{KCl}}) + \beta_{\{\mathrm{NaCl}\times\mathrm{KCl}\}}(f_{\mathrm{NaCl}}f_{\mathrm{KCl}}) + \beta_{\{\mathrm{KCl}\times\mathrm{K_2SO_4}\}}(f_{\mathrm{KCl}}f_{\mathrm{K_2SO_4}}) + \beta_{N_{\mathrm{salt}}}(N_{\mathrm{salt}}); 1 = \sum_{i=1}^{k} f_i,$$

where β is estimates, f is fraction of salt in mixture, and N is mole equivalents of salt used. Note that this equation excludes the standard error shown in Table 1 for simplicity. Furthermore, this linear model nor the other below should be regarded as perfect descriptions of the phenomena, rather as best estimations with the provided data. Based on experimental observations, smaller particle sizes are best suited to high specific capacity and high rate capability. Based on the model above, using 1 mol equivalent of salt, a mixture of 93.8% KCl and 6.2% NaCl (mp ≈ 747 °C) would yield a minimum d_{50} particle size of 3.08 μm; this was supported experimentally with a sample yielding a d_{50} particle size of 3.02 μm (see Fig. S19†). As a final note regarding particle size, the calcination temperature (880 °C) selected for these experiments is well above what is recommended for LNO synthesis,[56] therefore more practical temperatures will yield smaller particle sizes than those shown here. This does not discount the trends observed, as there should be no interaction between salt and temperature.

Another important factor when considering the capabilities of NCMs is the concentration of point defects, specifically Ni in

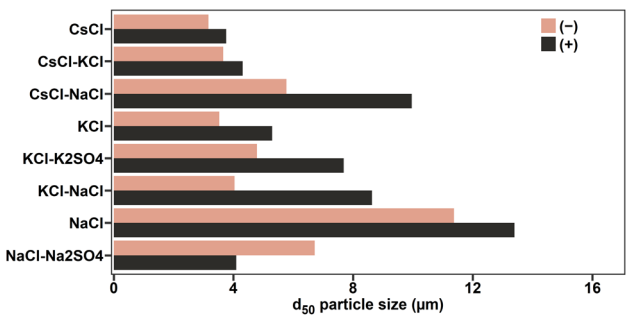

Fig. 2 Bar plot of d_{50} particle sizes for all samples prepared.

Table 1 Estimates of d_{50} particle size for statistically significant factors accompanied by their standard error and t-values

Factor	Estimate, β (μm)	Std. error (μm)	t-ratio	Prob > |t|
NaCl[a]	10.099	0.7793	12.96	<0.0001
KCl[a]	2.1141	0.8197	2.58	0.0275
NaCl × KCl	−9.1181	3.5780	−2.55	0.0289
KCl × K_2SO_4	11.432	4.8821	2.34	0.0412
Salt mol. ratio	1.0027	0.15291	6.56	<0.0001

[a] Due to the nature of a mixture design, the contribution of these factors is convolved with other main effect mixture factors.

the Li layer ($Ni^{\bullet}_{Li}$). When LNO is not synthesized under extremely oxidative conditions and the presence of stoichiometric Li, it results in Ni^{2+} residing in the Li layer (Wyckoff 3b) of the structure, since Li^{+} and Ni^{2+} have similar ionic radii of 0.76 Å and 0.69 Å, respectively.[56–58] Under most circumstances, $Ni^{\bullet}_{Li}$ can be regarded as a negative trait that diminishes specific capacity[53,59] and lithium diffusion (kinetics).[60,61] As a result, one's objective should be to minimize the defect concentration. As alluded to earlier, this can be achieved by synthesizing under flowing O_2, at lower temperatures, and with use of excess lithium reagents. Evaluation of the $Ni^{\bullet}_{Li}$ defect fraction was done *via* Rietveld refinement using GSAS II with a described fitting methodology outlined in Scheme S1† and whose results can be found in Table S3.† Fig. 3 shows representative refinements and X-ray diffraction (XRD) patterns as companion data to that shown in Fig. 1. From these refinements come the data represented in Fig. 4. As seen in Fig. 4, NaCl–Na_2SO_4(+) stands out as an anomaly among the others. This can also be observed in the general size trend between (−) and (+) counterparts in Fig. 2. The respective data point was excluded from all analysis models as an outlier, which seems to be caused by the synthetic inclusion of Na_2SO_4. Interestingly, this observation is in contradiction with past work on molten salt synthesis of $LiNi_{1/3}Co_{1/3}Mn_{1/3}O_2$ (NCM111).[44] One proposed underlying mechanism is related to the increased Ni content (100 *vs.* 33%) and its ability to diffuse through the molten salt and form LNO. First, the $Ni^{2+}SO_4^{2-}$ ionic association requires a simple 1 : 1 pairing relative to Co^{3+} and Mn^{4+}, which would need a second anion (Cl^- or SO_4^{2-}, respectively) and a more entropically demanding arrangement to balance charge and stabilize association. To minimize this entropic demand, Co^{3+} and Mn^{4+} would likely separate from the melt to integrate with nearby NCM particles. Second, LNO formation could be hindered due to the greater ionic radius of Ni^{2+} (0.69 Å) relative to Co^{3+} (0.545 Å) and Mn^{4+} (0.53 Å), which could lead to more limited Brownian diffusion in the melt, thus crystal growth during synthesis. Regardless, other work[62] notes that materials with $Ni^{\bullet}_{Li}$ fractions greater than 10%, as seen in Fig. 4 for NaCl–Na_2SO_4(+), have suppressed particle growth, which deviates from more stoichiometric samples, as seen in Fig. 2, and from comparison of NaCl–Na_2SO_4(−) and NaCl–Na_2SO_4(+) particles in Fig. S16 and S17.†

Disregarding the outlier, a model has been constructed identifying statistically significant factors for crystalline quality. Interestingly, molar salt ratio is not a critical factor. This contrasts with comments in past work that expressed concern about high molten salt ratios physically blocking oxidative species (O_2) from reacting with forming LNO.[40] This does not mean that salt ratio has no effect, but rather that no significant effect is found for the molar ratios selected for this design. As for significant factors, the set can be broken down into "pure chlorides", which have varying differences in defect concentration contributions, with KCl being most favorable to well-ordered LNO, while the second set contains sulfate salts, which have a deleterious effect on crystalline quality for reasons noted earlier. A full model is shown in the following equation (see also Table 2):

$$\%Ni_{Li} = \beta_{NaCl} f_{NaCl} + \beta_{KCl} f_{KCl} + \beta_{CsCl} f_{CsCl} + \beta_{\{NaCl\times Na_2SO_4\}} f_{NaCl} f_{Na_2SO_4} + \beta_{\{KCl\times K_2SO_4\}} f_{KCl} f_{K_2SO_4};$$

$$1 = \sum_{i=1}^{k} f_i.$$

The last factors examined were experimental effects on particle size distribution (PSD), as well as the effect of molten salt volume on each investigated feature. To illustrate the importance of minimal PSD, consider two sets of particles with the same d_{50} size, yet one is perfectly uniform, while the other has a broad PSD. The broad PSD set is subject to non-uniform charging kinetics (charge heterogeneity), leading to possible degradation and decreased

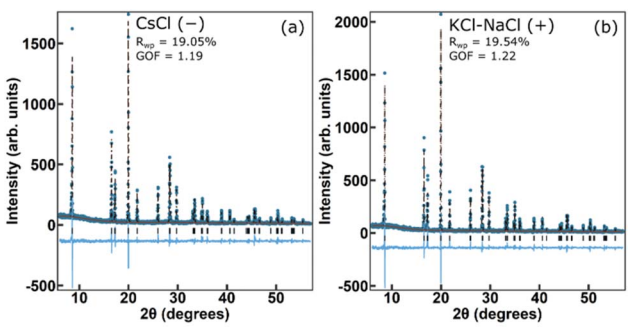

Fig. 3 Rietveld refined XRD patterns of representative samples, (a) CsCl(−) and (b) KCl–NaCl(+). Patterns of other representative samples can be found in Fig. S20–S36.†

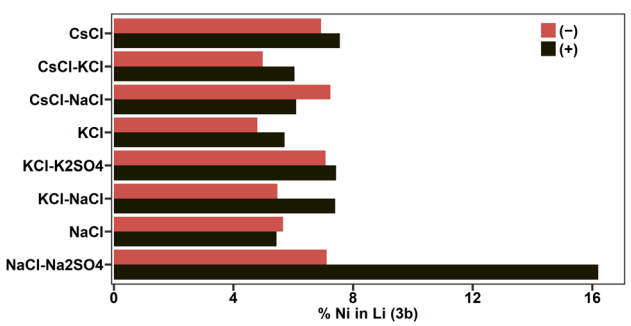

Fig. 4 Bar plot of $Ni^{\bullet}_{Li}$ defect fraction for all samples prepared.

Table 2 Estimates of $Ni^{\bullet}_{Li}$ defect fraction for statistically significant factors accompanied by their standard error and *t*-values

Factor	Estimate, β (%)	Std. error (%)	*t*-ratio	Prob > |*t*|
NaCl[a]	6.0155	0.47361	12.70	<0.0001
KCl[a]	5.3155	0.47361	11.22	<0.0001
CsCl[a]	7.0015	0.47361	14.78	<0.0001
NaCl × Na_2SO_4	15.586	3.3833	4.61	0.0010
KCl × K_2SO_4	17.431	3.5642	4.89	0.0006

[a] Due to the nature of a mixture design, the contribution of these factors is convolved with other main effect mixture factors.

capacity[25,63,64] (deviations in relative ratio of surface-region material and bulk material results in uneven degradation),[65] and this distribution of particle sizes further determines how much coating or doping content a material needs for optimal performance. In contrast, a perfectly uniform particle size provides predictable performance and behavior. With this in mind, particle span was analyzed using SEM image analysis methods described in the ESI.† While the three chlorides (Na, K, Cs) were statistically significant, the estimates for span did not vary much between one another (Fig. S37 and Table S4†). NaCl–Na_2SO_4 was found to be very negative to narrow PSD, however is already discounted for the aforementioned reasons. Therefore, no greater insights can be extracted from salt selection with the given data. Molten salt volume was an uncontrolled factor that may have had an effect on particle size, $Ni^{\bullet}_{Li}$, and PSD based on the hypothesis that simple volume of molten salt with respect to the reagents, rather than any specific salt, is significant. Linear regressions of each observed feature with respect to estimated molten salt volume (Fig. S38–S40†)[66] found no significant correlations ($R^2 \leq 0.115$).

To summarize, we explored an experimental design of select molten salt mixtures at different molar ratios to $Ni(OH)_2$ to identify what effect these common factors have on critical features for SC-LNO synthesis. Regarding particle size, molar salt ratio had a significant, albeit modest positive effect on particle size, while NaCl was found to have a large and significant effect on particle size. This stands in contrast with KCl whose presence yields small particles and has a negative second-order interaction with NaCl. On the other hand, the effect of $Ni^{\bullet}_{Li}$ defect fraction in LNO is simpler, where the chloride salts tested had varying contributions, with KCl-derived samples having a more ordered crystal structure than their counterparts (use of sulfate salts leads to deleterious effects on structure quality). Lastly, particle size dispersity was considered, however no substantial claims can be made even with significant factors. This also holds true for correlations between molten salt volume and any aforementioned particle feature.

Author contributions

Wessel van den Bergh: conceptualization, data curation, formal analysis, investigation, methodology, writing – original draft, visualization, software, writing – review & editing; Rui Yao: investigation; Ruizhuo Zhang: investigation; Aleksandr Kondrakov: supervision, writing – review & editing; Jürgen Janek: supervision, writing – review & editing; Torsten Brezesinski: funding acquisition, supervision, project administration, validation, visualization, writing – review & editing.

Conflicts of interest

There are no conflicts to declare.

Acknowledgements

This work was supported by BASF SE. The authors are grateful to the Federal Ministry of Education and Research (Bundesministerium für Bildung und Forschung, BMBF) for funding within the project UNIKAM (03XP0484B). The authors also thank Sabrina Sicolo (BASF SE) for helpful discussions.

References

1 *National Blueprint for Lithium Batteries 2021–2030*, U.S. Department of Energy, 2021.
2 D. Baek, A. Bocca and A. Macii, *Energy, Ecol. Environ.*, 2022, **7**, 604–613.
3 L. Mauler, F. Duffner, W. G. Zeier and J. Leker, *Energy Environ. Sci.*, 2021, **14**, 4712–4739.
4 A. Mukherji, P. Thorne, W. W. L. Cheung, S. L. Connors, M. Garschagen, O. Geden, B. Hayward, N. P. Simpson, E. Totin, K. Blok, S. Eriksen, E. Fischer, G. Garner, C. Guivarch, M. Haasnoot, T. Hermans, D. Ley, J. Lewis, Z. Nicholls, L. Niamir, S. Szopa, B. Trewin, M. Howden, C. Méndez, J. Pereira, R. Pichs, S. K. Rose, Y. Saheb, R. Sánchez, C. Xiao and N. Yassaa, *AR6 Synthesis Report: Climate Change 2023*, IPCC, 2023.
5 F. Creutzig, L. Niamir, X. Bai, M. Callaghan, J. Cullen, J. Díaz-José, M. Figueroa, A. Grubler, W. F. Lamb, A. Leip, E. Masanet, É. Mata, L. Mattauch, J. C. Minx, S. Mirasgedis, Y. Mulugetta, S. B. Nugroho, M. Pathak, P. Perkins, J. Roy, S. de la Rue du Can, Y. Saheb, S. Some, L. Steg, J. Steinberger and D. Ürge-Vorsatz, *Nat. Clim. Change*, 2022, **12**, 36–46.
6 M. Wentker, M. Greenwood and J. Leker, *Energies*, 2019, **12**, 504.
7 W. Li, E. M. Erickson and A. Manthiram, *Nat. Energy*, 2020, **5**, 26–34.
8 J. B. Goodenough and Y. Kim, *Chem. Mater.*, 2010, **22**, 587–603.
9 K. Mizushima, P. C. Jones, P. J. Wiseman and J. B. Goodenough, *Mater. Res. Bull.*, 1980, **15**, 783–789.
10 Y. Kim, W. M. Seong and A. Manthiram, *Energy Storage Mater.*, 2021, **34**, 250–259.
11 G. A. Campbell, *Miner. Econ.*, 2020, **33**, 21–28.
12 H.-J. Noh, S. Youn, C. S. Yoon and Y.-K. Sun, *J. Power Sources*, 2013, **233**, 121–130.
13 M. S. Whittingham, *Chem. Rev.*, 2004, **104**, 4271–4302.
14 W. W. Dlamini, G. Nelson, S. S. Nielsen and B. A. Racette, *Am. J. Ind. Med.*, 2020, **63**, 36–43.
15 M. Bianchini, M. Roca-Ayats, P. Hartmann, T. Brezesinski and J. Janek, *Angew. Chem., Int. Ed.*, 2019, **58**, 10434–10458.
16 R. Jung, M. Metzger, F. Maglia, C. Stinner and H. A. Gasteiger, *J. Phys. Chem. Lett.*, 2017, **8**, 4820–4825.
17 T. Li, X.-Z. Yuan, L. Zhang, D. Song, K. Shi and C. Bock, *Electrochem. Energy Rev.*, 2020, **3**, 43–80.
18 S.-Y. Lee, G.-S. Park, C. Jung, D.-S. Ko, S.-Y. Park, H. G. Kim, S.-H. Hong, Y. Zhu and M. Kim, *Adv. Sci.*, 2019, **6**, 1800843.
19 K.-J. Park, J.-Y. Hwang, H.-H. Ryu, F. Maglia, S.-J. Kim, P. Lamp, C. S. Yoon and Y.-K. Sun, *ACS Energy Lett.*, 2019, **4**, 1394–1400.
20 J. R. Dahn, E. W. Fuller, M. Obrovac and U. von Sacken, *Solid State Ionics*, 1994, **69**, 265–270.
21 K. Xu, *Chem. Rev.*, 2004, **104**, 4303–4418.
22 J. Li and A. Manthiram, *Adv. Energy Mater.*, 2019, **9**, 1902731.

23 L. Kong, C. Li, J. Jiang and M. G. Pecht, *Energies*, 2018, **11**, 2191.
24 S. Hess, M. Wohlfahrt-Mehrens and M. Wachtler, *J. Electrochem. Soc.*, 2015, **162**, A3084–A3097.
25 E. Trevisanello, R. Ruess, G. Conforto, F. H. Richter and J. Janek, *Adv. Energy Mater.*, 2021, **11**, 2003400.
26 P. Minnmann, L. Quillman, S. Burkhardt, F. H. Richter and J. Janek, *J. Electrochem. Soc.*, 2021, **168**, 040537.
27 R. Ruess, S. Schweidler, H. Hemmelmann, G. Conforto, A. Bielefeld, D. A. Weber, J. Sann, M. T. Elm and J. Janek, *J. Electrochem. Soc.*, 2020, **167**, 100532.
28 S. Payandeh, D. Goonetilleke, M. Bianchini, J. Janek and T. Brezesinski, *Curr. Opin. Electrochem.*, 2022, **31**, 100877.
29 S. Payandeh, C. Njel, A. Mazilkin, J. H. Teo, Y. Ma, R. Zhang, A. Kondrakov, M. Bianchini and T. Brezesinski, *Adv. Mater. Interfaces*, 2023, **10**, 2201806.
30 P. Minnmann, F. Strauss, A. Bielefeld, R. Ruess, P. Adelhelm, S. Burkhardt, S. L. Dreyer, E. Trevisanello, H. Ehrenberg, T. Brezesinski, F. H. Richter and J. Janek, *Adv. Energy Mater.*, 2022, **12**, 2201425.
31 J. Langdon and A. Manthiram, *Energy Storage Mater.*, 2021, **37**, 143–160.
32 D. Pritzl, T. Teufl, A. T. S. Freiberg, B. Strehle, J. Sicklinger, H. Sommer, P. Hartmann and H. A. Gasteiger, *J. Electrochem. Soc.*, 2019, **166**, A4056–A4066.
33 T.-J. Park, J.-B. Lim and J.-T. Son, *Bull. Korean Chem. Soc.*, 2014, **35**, 357–364.
34 J. Li, H. Li, W. Stone, R. Weber, S. Hy and J. R. Dahn, *J. Electrochem. Soc.*, 2017, **164**, A3529–A3537.
35 T. Pan, J. Alvarado, J. Zhu, Y. Yue, H. L. Xin, D. Nordlund, F. Lin and M. M. Doeff, *J. Electrochem. Soc.*, 2019, **166**, A1964–A1971.
36 B. Huang, M. Wang, Y. Zuo, Z. Zhao, X. Zhang and Y. Gu, *Solid State Ionics*, 2020, **345**, 115200.
37 R. Rueß, D. Gomboso, M. Ulherr, E. Trevisanello, Y. Ma, A. Kondrakov, T. Brezesinski and J. Janek, *J. Electrochem. Soc.*, 2023, **170**, 020533.
38 H. Li, J. Li, N. Zaker, N. Zhang, G. A. Botton and J. R. Dahn, *J. Electrochem. Soc.*, 2019, **166**, A1956–A1963.
39 F. Li, L. Kong, Y. Sun, Y. Jin and P. Hou, *J. Mater. Chem. A*, 2018, **6**, 12344–12352.
40 A. Mesnier and A. Manthiram, *ACS Appl. Mater. Interfaces*, 2023, **15**, 12895–12907.
41 M. Kim, L. Zou, S.-B. Son, I. D. Bloom, C. Wang and G. Chen, *J. Mater. Chem. A*, 2022, **10**, 12890–12899.
42 G. Qian, Y. Zhang, L. Li, R. Zhang, J. Xu, Z. Cheng, S. Xie, H. Wang, Q. Rao, Y. He, Y. Shen, L. Chen, M. Tang and Z.-F. Ma, *Energy Storage Mater.*, 2020, **27**, 140–149.
43 M. Kim, J. Zhu, L. Li, C. Wang and G. Chen, *ACS Appl. Energy Mater.*, 2020, **3**, 12238–12245.
44 T. Kimijima, N. Zettsu and K. Teshima, *Cryst. Growth Des.*, 2016, **16**, 2618–2623.
45 Y. Kim, *ACS Appl. Mater. Interfaces*, 2012, **4**, 2329–2333.
46 C. Sikalidis and T. Kimura, in *Advances in Ceramics – Synthesis and Characterization, Processing and Specific Applications*, IntechOpen, 2011.
47 D. E. Bugaris and H.-C. zur Loye, *Angew. Chem., Int. Ed.*, 2012, **51**, 3780–3811.
48 W. van den Bergh, H. N. Lokupitiya, N. A. Vest, B. Reid, S. Guldin and M. Stefik, *Adv. Funct. Mater.*, 2021, **31**, 2007826.
49 M. Doyle and J. Newman, *J. Appl. Electrochem.*, 1997, **27**, 846–856.
50 M. Weiss, R. Ruess, J. Kasnatscheew, Y. Levartovsky, N. R. Levy, P. Minnmann, L. Stolz, T. Waldmann, M. Wohlfahrt-Mehrens, D. Aurbach, M. Winter, Y. Ein-Eli and J. Janek, *Adv. Energy Mater.*, 2021, **11**, 2101126.
51 Y. Kim, H. Kim and A. Manthiram, *J. Power Sources*, 2023, **558**, 232633.
52 P. Kurzhals, F. Riewald, M. Bianchini, H. Sommer, H. A. Gasteiger and J. Janek, *J. Electrochem. Soc.*, 2021, **168**, 110518.
53 F. Riewald, P. Kurzhals, M. Bianchini, H. Sommer, J. Janek and H. A. Gasteiger, *J. Electrochem. Soc.*, 2022, **169**, 020529.
54 W. van den Bergh, L. Karger, S. Murugan, J. Janek, A. Kondrakov and T. Brezesinski, *ChemElectroChem*, 2023, **10**, e202300165.
55 K. Oura, M. Katayama, A. V. Zotov, V. G. Lifshits and A. A. Saranin, in *Surface Science: An Introduction*, ed. K. Oura, M. Katayama, A. V. Zotov, V. G. Lifshits and A. A. Saranin, Springer, Berlin, Heidelberg, 2003, pp. 229–260.
56 M. Bianchini, F. Fauth, P. Hartmann, T. Brezesinski and J. Janek, *J. Mater. Chem. A*, 2020, **8**, 1808–1820.
57 M. Bianchini, J. Wang, R. J. Clément, B. Ouyang, P. Xiao, D. Kitchaev, T. Shi, Y. Zhang, Y. Wang, H. Kim, M. Zhang, J. Bai, F. Wang, W. Sun and G. Ceder, *Nat. Mater.*, 2020, **19**, 1088–1095.
58 R. D. Shannon, *Acta Crystallogr.*, 1976, **32**, 751–767.
59 S. Sicolo, M. Sadowski, K. Vettori, M. Bianchini, J. Janek and K. Albe, *Chem. Mater.*, 2024, **36**, 492–500.
60 N. Phattharasupakun, M. M. E. Cormier, E. Lyle, E. Zsoldos, A. Liu, C. Geng, Y. Liu, H. Li, M. Sawangphruk and J. R. Dahn, *J. Electrochem. Soc.*, 2021, **168**, 090535.
61 P. Xiao, N. Zhang, H. S. Perez and M. Park, *arXiv*, 2023, preprint, arXiv:2311.06140 [cond-mat.mtrl-sci], DOI: **10.48550/arXiv.2311.06140**.
62 D. Goonetilleke, B. Schwarz, H. Li, F. Fauth, E. Suard, S. Mangold, S. Indris, T. Brezesinski, M. Bianchini and D. Weber, *J. Mater. Chem. A*, 2023, **11**, 13468–13482.
63 J. Park, H. Zhao, S. D. Kang, K. Lim, C.-C. Chen, Y.-S. Yu, R. D. Braatz, D. A. Shapiro, J. Hong, M. F. Toney, M. Z. Bazant and W. C. Chueh, *Nat. Mater.*, 2021, **20**, 991–999.
64 Y. Bi, J. Tao, Y. Wu, L. Li, Y. Xu, E. Hu, B. Wu, J. Hu, C. Wang, J.-G. Zhang, Y. Qi and J. Xiao, *Science*, 2020, **370**, 1313–1317.
65 Y. Song, X. Wang, H. Cui, J. Huang, Q. Hu, X. Xiao, H. Liang, K. Yang, A. Wang, J. Liu, H. Huo, L. Wang, Y. Gao and X. He, *eTransportation*, 2023, **16**, 100223.
66 G. J. Janz, *Thermodynamic and Transport Properties for Molten Salts: Correlation Equations for Critically Evaluated Density, Surface Tension, Electrical Conductance, and Viscosity Data*, American Chemical Society; American Institute of Physics, New York, 1988.

